A seismic signature of river bedload transport during storm events

Leslie Hsu,[1,2] Noah J. Finnegan,[1] and Emily E. Brodsky[1]

Received 12 April 2011; revised 3 June 2011; accepted 3 June 2011; published 14 July 2011.

[1] Seasonal patterns in high frequency seismic waves near rivers can record energy transmitted to the river bed from particle impacts during bedload transport. Here we show that single storm events in a river can also be observed seismically. We analyzed the high frequency seismic noise in a reach of the Cho-Shui (Zhuóshuǐ) River in central Taiwan and made detailed observations during individual storm events. Discharge, derived from a water level gage 4.25 km from the seismometer, is highly variable due to typhoons. We found a correlation between seismic amplitude and discharge that differs on the rising and falling limbs of three storms. During each storm, for a given discharge the amplitude of seismic waves are on average two times greater on the rising limb of the storm than on the falling limb, in both aggradational and erosional events. Clockwise hysteresis in both aggradational and erosional events implies that water turbulence, alone, is not the source of the seismic waves. If seismic wave amplitude correlates linearly with the flux of bedload, this implies a roughly two-fold decrease in transport efficiency over the time-scale of days during individual storms. The observed change in transport efficiency can plausibly be explained by the disturbance of bed armor during storms and subsequent reformation during the waning stages. This data highlights the potential for fluvial seismology to reveal the dynamics of bedload transport. **Citation:** Hsu, L., N. J. Finnegan, and E. E. Brodsky (2011), A seismic signature of river bedload transport during storm events, *Geophys. Res. Lett.*, *38*, L13407, doi:10.1029/2011GL047759.

1. Introduction

[2] Gravel and cobble transport by rivers governs channel change, and is therefore of great importance to geomorphologists and river engineers. The most commonly used approaches to estimating bedload transport rates are empirically calibrated relationships based on flume experiments [e.g., *Meyer-Peter and Müller*, 1948; *Wilcock and Crowe*, 2003]. However, it is difficult to assess how effectively such relationships predict transport rates during extreme events in large rivers because quantitative measures of bedload transport are labor intensive and, at high flows, often dangerous to obtain. For logistical reasons, most bedload studies have been carried out in small mountain streams.

[3] Particle impacts on the river bed transfer momentum, which in turn generates elastic (seismic) waves. Therefore, seismology can potentially constrain bedload transport rates in rivers. High frequency (>1 Hz) seismic waves have been used to study earth surface processes such as ocean waves [*Adams et al.*, 2002], landslides [*Favreau et al.*, 2010], rockfalls [*Deparis et al.*, 2008], debris flows [*LaHusen*, 2005; *Suwa et al.*, 2003; *Burtin et al.*, 2009], and snow avalanches [*Vilajosana et al.*, 2007; *Cole et al.*, 2009]. In all of these cases, remote monitoring is possible because geophones or seismometers capture ground vibrations caused by the surface process. A few studies have used seismological data to study fluvial processes [e.g., *Govi et al.*, 1993], and recent work showed that high frequency seismic waves may provide a way to monitor bedload sediment transport in inaccessible rivers in the Himalaya. *Burtin et al.* [2008] showed that seismic wave amplitude along the Trisuli River in Nepal correlated well with hydrological processes such as daily precipitation and river discharge cycles. In addition, over the year of available data, the seismic amplitude was greater for a given river stage at the start of the Indian Monsoon than at the end. This was interpreted as evidence for a bedload source for seismic waves, as opposed to water turbulence, because significant hysteresis is not expected in the relationship between stage and turbulence, whereas hysteresis is common in sediment rating curves. However, in addition to sediment supply, many other factors (e.g., bed armoring, channel geometry) might influence the relationship between river stage and the amplitude of ground vibrations.

[4] In this paper we move closer to a direct connection between bedload transport and seismic wave amplitude by studying one site on the Cho-Shui River in Taiwan that has experienced repeated, short-lived, and quantitatively-documented typhoons. This dataset combines nearby water level, channel cross-section, discharge, and seismic amplitude measurements from existing infrastructure. A major goal of our work is to determine if a consistent, time-varying relationship between the amplitude of ground vibrations and river flux holds during multiple events. By examining several events with different durations and intensities, we show that during each storm there is a clear distinction between the seismic amplitudes generated for a given water discharge as the water rises compared to when it falls. Whether the event is aggradational or erosional, there is a greater amplitude of seismic noise at the beginning of the storm in all three typhoon events. This key observation combined with a contrasting observation for smaller subevents and simple hydraulic arguments suggests that bedload transport controls the seismic wave generation. Furthermore, the observed hysteresis is consistent with an increase in the threshold stress for sediment entrainment during each event caused by packing and/or coarsening of the alluvial bed.

2. Site and Methods

[5] The study site on the Cho-Shui River in Taiwan was selected because it has highly variable water discharge, high

[1]Department of Earth and Planetary Sciences, University of California, Santa Cruz, California, USA.
[2]Now at Lamont-Doherty Earth Observatory, Palisades, New York, USA.

0094-8276/11/2011GL047759

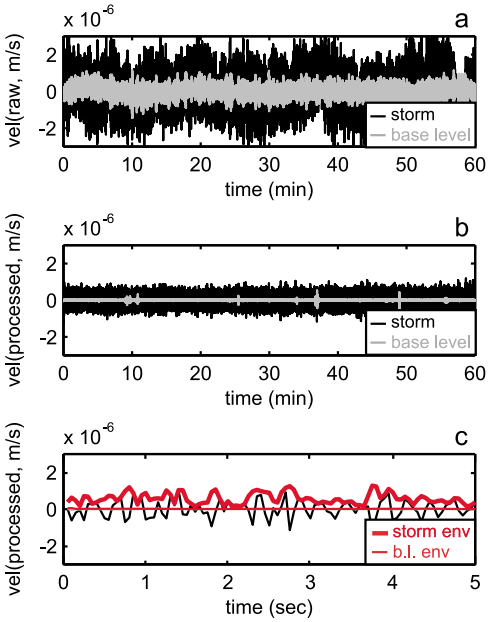

Figure 1. Illustration of the seismic processing steps, showing the difference between raw, filtered, and envelope values for storm and non-storm data. (a) Raw seismic velocity data (m/s) recorded at station SSLB for two different conditions: Black line: during the peak of Typhoon Morakot (10 August 2009) and gray line: base level flow one week before the storm (3 August 2009). (b) 1–9 Hz band filtered data for the same time period, showing the high frequency component of the signal linked to river processes. (c) The envelope (Hilbert function – a measure of the power in the signal over time) is shown by the red lines, (storm: thick red line; base level: thin red line, which covers the grey line at this resolution.) Note that the amplitude of the seismic velocity is much larger during the storm than during the background base level flow.

sediment supply, available high frequency seismic wave measurements from a broadband seismometer, and available water level and discharge data derived from a gaging station. At the site, the river is gravel-bedded within a bedrock canyon. The local channel width is 200 m and the local reach bed slope is 0.005 (Figure S1 of the auxiliary material).[1]

[6] The seismic station SUANG-LONG (SSLB of the Broadband Array in Taiwan for Seismology, 23.7875N, 120.9540E) is located ~50 meters from the edge of the river. It includes an STS-2 sensor that collects broadband data at 20 Hz sampling frequency. The water station (1510H075, Bao-shih Bridge, 23.7942N, 120.9142E) is 4.25 km downstream of the seismometer, and records hourly water level. Water discharge is calculated from river stage combined with measured cross sections [*Water Resources Planning Commission*, 2008, 2009]. The channel bed here is dynamic; the channel elevation at a specific point in the cross sectional profile may change by meters from storm to storm (Figure S2). The variable channel geometry leads to complexities in the rating curves, which relate water level and discharge (Figure S3). While the water level value is a raw measurement without any interpretation, if aggradation or erosion has occurred, its unit of meters above sea level (m.a.s.l.) does not necessarily translate directly to local water depth. In contrast, the derived discharge measurement is calculated with a rating curve and should account for bed elevation change, however the accuracy of the rating curve is uncertain in highly dynamic reaches. Consequently, we use both the water level and discharge datasets accordingly in our analysis.

[7] We examined the high frequency content of the seismic noise, which was previously shown to link to river processes [*Burtin et al.*, 2008]. We extracted the 1–9 Hz band, then calculated the envelope with a Hilbert transform. Figure 1 shows the distinctions between the raw signal, the bandpassed signal, and the envelope function. We used an hourly average of the envelope function to compare with the hourly water data. We analyzed seismic amplitude and water data from the entire year 2008, which had several storm events, and the one large storm in 2009, Typhoon Morakot.

3. Results: Hysteresis in the Relationships Between Seismic Amplitude Versus Water Level and Seismic Amplitude Versus Discharge

[8] The time series for seismic wave amplitude and water level closely track each other on the rising limb, but decrease at different rates on the falling limb. Figures 2a–2c show this close relationship for the three storms with complete seismic records, Events 2008a, 2008b, and 2009a (Morakot), respectively. (A fourth storm, Event 2008c, shows the same patterns but has a significant gap in the seismic record. It is shown in Figure S4.) At the beginning of the flood hydrograph, the increase in seismic amplitude occurs immediately, within one hour (one timestep) of the increase in water level. However, the relationship between seismic amplitude and water level differs on the rising and falling limbs of the storms. After the peak water level, the seismic noise decays at a faster rate, reaching the initial base level values before the water level returns to base level. This creates a clockwise hysteresis effect in seismic amplitude as a function of water level (Figures 2d–2f).

[9] The same patterns are observed in the time series of seismic wave amplitude and water discharge. They closely follow each other on the rising limb of storms, with both discharge and seismic amplitude increasing sharply (Figures 2g–2i). On the falling limb, the seismic amplitude decreases faster than the water discharge. For a given discharge, the ratio of the seismic amplitude on the rising limb to the amplitude on the falling limb is about two (see auxiliary material for more details). Note that the two smaller discharge peaks (one on the falling limb of Event 2008b in Figure 2b, and one on the rising limb of Event 2009a in Figure 2c) do not exhibit the clockwise hysteresis. The peak on the falling limb of Event 2008b actually displays counter-clockwise hysteresis (Figure 2e, 2k, insets). These subevents are smaller both in magnitude (the peak discharge is much lower, by almost an order of magnitude) and duration (they last for a day or less, instead of a week or more). Also, for the subevent on the falling limb, the initial condition of the bed is different from the condition for large events because the pre-subevent discharge is not as low as pre-storm base level. The entire dataset, which shows the

[1] Auxiliary materials are available in the HTML. doi:10.1029/2011GL047759.

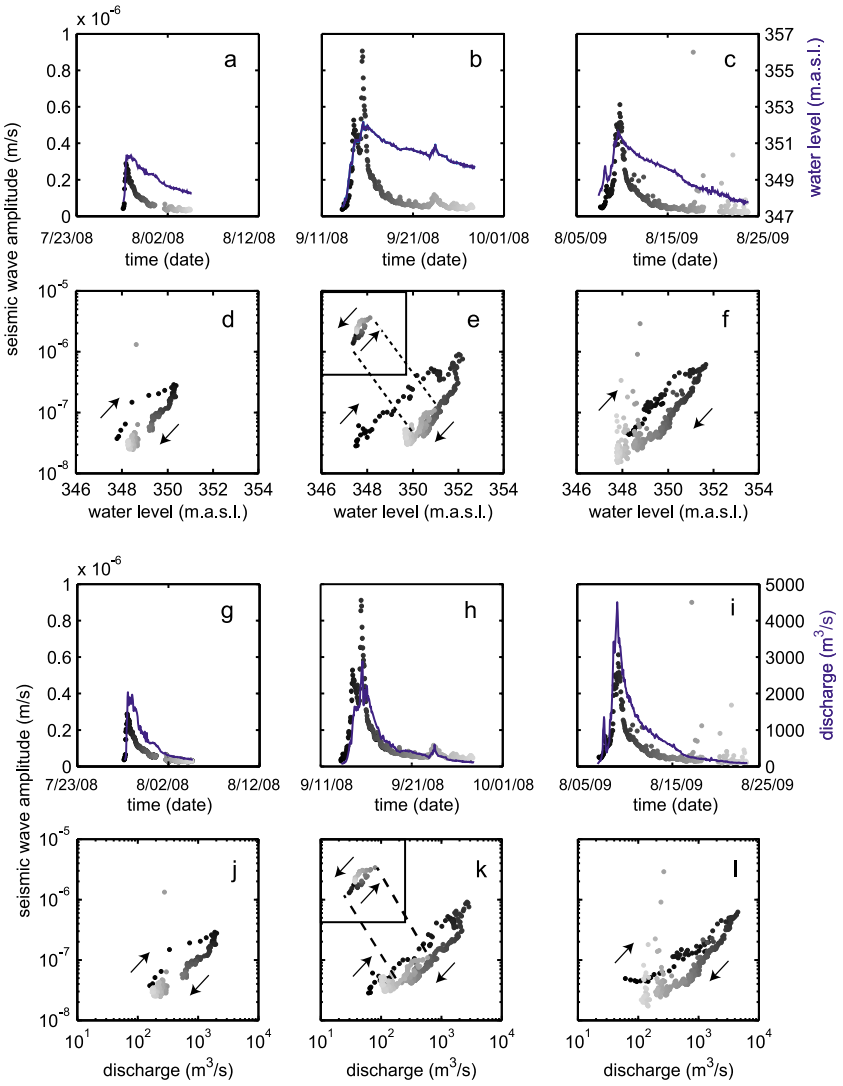

Figure 2. Relationships between seismic wave amplitude, water level, and discharge. We show the three events with a complete seismic record, (a) Event 2008a, (b) Event 2008b, (c) Event 2009a (Typhoon Morakot) – each entire column corresponds to the same event. (a–c) Seismic wave amplitude (m/s, left axis, gray-gradient dots becoming lighter with time) and water level (meters above sea level, blue line) versus time (date). The water level curves suggest channel aggradation in Figures 2a and 2b, but erosion in Figure 2c. (d–f) Seismic wave amplitude vs. water level corresponding to events 2008a, 2008b, and 2009a, respectively. Gray gradient showing temporal evolution matches that in Figures 2a–2c. Arrows indicate the clockwise hysteresis. (e) The inset shows that the small peak on the falling limb of 2008b exhibits counter-clockwise hysteresis. The inset scale is the same as in the main panel – the subset is simply translated – but the inset shading was rescaled to the sub-period to better show the sense of the hysteresis. (f) The abnormally high values in Event 2009a are due to seismicity from earthquakes. (g–l) Same as (a–f) but for discharge (m^3/s) instead of water level.

events in the context of preceding and subsequent data, is shown in Figure S5.

4. The Source of Seismic Waves

[10] We are measuring energy transferred from the river to the bed due to either fluid turbulence or impacting bedload particles. In order to link the seismic signal to sediment transport processes, it is necessary to first determine which of these scenarios is more likely. Towards this end, we use our data to test end-member hypotheses for the source of the seismic noise by exploring each of their predictions of the hysteresis.

[11] Hysteresis could occur in the absence of bedload-generated seismic waves by two distinct processes. First, hysteresis can result from the fact that on the rising limb of a flood, the flood wave drives a pressure gradient in the direction of the river flow, whereas on the falling limb the water surface generates a pressure gradient that opposes the river flow. This means that for the same stage, a higher velocity (and therefore discharge) is observed on the rising limb than on the falling limb. Second, hysteresis can be generated by a change in bed shape due to erosion or aggradation that causes a change in stage-discharge relationships during a storm. Alternatively, if sediment transport generates the seismic waves, hysteresis can be linked to either

supply limitation during the event [e.g., *Leopold and Emmett*, 1977] or bed armor destruction and reformation [e.g., *Reid et al.*, 1985]. These distinct predictions of the source of hysteresis provide a tool to distinguish between the sources of the seismic waves.

[12] If turbulent dissipation is the source of seismic amplitude, we expect a linear scaling between shaking and discharge [e.g., *Burtin et al.*, 2008]. This is because turbulence should depend most directly on the rate of dissipation of potential energy via turbulence, or in other words, river power. River power, for a given slope and cross-section, depends linearly on discharge under steady and uniform flow. Thus if the observed hysteresis is related to the water surface pressure gradient effect articulated above, then the 2-fold reduction in seismic amplitude on the falling limb compared to the rising limb should correspond to a 2-fold reduction in discharge on the falling limb compared to the rising limb. For the most clearly resolved rising hydrograph limbs in the observed storms, stage changes by ~5 m over a time-scale, τ, of ~8 hours. Assuming this rise occurs from the downstream translation of a flood wave of height h at velocity u, the slope of the wave front, S_w, can be computed by:

$$S_w = h/(u\tau) \quad (1)$$

For a conservatively low estimate of the average flow velocity during a flood (2 m/s), the downstream water surface slope, S_w, needed to explain the magnitude of water rise during a storm is approximately 9×10^{-5} m/m, or roughly 1/60 the bed slope for the reach examined. This ~2% increase in the driving stress of a river from the flood wave is insufficient to explain the 2-fold higher magnitude of the seismic amplitude (and thus inferred discharge) on the rising limb. Thus, water surface pressure gradients are not likely to be the source of the hysteresis.

[13] To explain the sign of the observed hysteresis in all of typhoons examined, net channel bed aggradation would be required during each storm so that more water would be conveyed for a given water surface elevation on the rising limb as compared to the falling limb. Between 2008 and 2009, however, we observe significant incision of the channel (Figure S2). During Event 2009a, roughly 0.7 m of bed incision occurred at the gage (Figures 2c and S5b). Nevertheless, the sense of hysteresis in the relationship between seismic wave amplitude and discharge is the same for this event as in net aggradational events 2008a and 2008b. Since the data supports neither of the potential hysteresis effects associated with turbulence in the water column being the sole source of seismic waves, we conclude that bedload transport must be a contributor to seismic wave generation.

[14] Source limitation is a documented cause of hysteresis in bedload transport during events in nature [e.g., *Leopold and Emmett*, 1977; *Moog and Whiting*, 1998]. At a given reach during the course of an event, the sediment fraction mobilized by the shear stress of the flow may be depleted. The supply is built up again during low flows. At this site in the Cho-Shui river, source limitation is unlikely due to the abundant sediment supply. In addition, the storms we analyzed in 2008 follow each other immediately, leaving little time to replenish the sediment. Therefore source limitation cannot be the explanation for the hysteresis in all events. In addition, because the gravel transport distances for a storm are typically small relative to the length of a river [e.g., *Goff and Ashmore*, 1994], we focus on local (as opposed to source) effects as an explanation for the inferred reduction in transport efficiency.

[15] The second mechanism for hysteresis caused by bedload transport involves bed armor destruction and reformation. The state of the bed, for example grain size and packing density, can change over the course of a storm event. For a given bed stress, coarsening or packing of the bed should translate directly into a reduction in transport efficiency [e.g., *Reid et al.*, 1985; *Wilcock and Crowe*, 2003; *Gran and Montgomery*, 2005; *Turowski et al.*, 2011]. Thus changes in the packing density or grain size of the bed might provide a simple explanation for the observed hysteresis.

[16] The conceptual picture is a pre-storm bed that is armored, but this densely-packed state is destroyed during the early part of the rising limb, exposing an un-armored bed that will mobilize more readily at a given shear stress. As the flood peak wanes, the armor reforms (due to selective transport of finer grains or progressive packing of the bed) bringing the bed back to a more stable arrangement. Here we make a simplifying assumption that bedload flux is linearly related to the amplitude of seismic shaking, and we consider only saltating particles that achieve terminal velocity before impact. Then for the characteristic grain size sampled by our signal, impact energy should scale with the number of impacting particles, i.e., the bedload flux. Since the amplitude of seismic waves is linearly proportional to the impact force at the source [*Aki and Richards*, 2002, equation 4.26], it follows that seismic amplitude should scale linearly with transport rate under the simplifying conditions described above. The observed hysteresis thus implies, on average, a two-fold reduction in transport rate for a given discharge during each storm. Rolling or dragging contacts between particles are expected to have a smaller contribution to seismic noise (less energy transfer) than collisions, so if these interactions make up some fraction of the moving bedload, the same seismic wave amplitude would be caused by a larger flux of bedload than we assume. If the fraction of total bedload that is rolling or dragging is the same on the rising and falling limbs, then there is no change to the two-fold reduction in transport rate. If bedload transport has a greater fraction of these less-energetic rolling or dragging contacts on the falling limb, then a greater bedload flux occurs for the same seismic energy level, and the reduction in transport rate would be an overestimate.

[17] Both experiments [*Charru et al.*, 2004] and observations [*Reid et al.*, 1985] show substantial changes in transport rates for a given stage simply due to changes in the packing and/or grain size of the bed. Thus the observed hysteresis is consistent with a bedload source for seismic amplitude. Moreover, our results indicate that on the Cho-Shui River, changes in the efficiency of bedload transport follow a similar trajectory from large storm to large storm, regardless of whether there is net aggradation or erosion. Although it is possible that both water and bedload contribute to the observed shaking, our results indicate that bedload is the dominant component of the seismic source.

[18] A possible explanation for why the smaller subevents do not exhibit the same hysteresis as the typhoons is that these events have different initial conditions compared to the large

events. For example, *Reid et al.* [1985] demonstrated that the delay between the hydrograph peak and the bedload transport peak on a creek in England was controlled primarily by how consolidated the bed was. Transport events that took place when the bed was consolidated resulted in peaks in gravel transport on the recessional limb of the hydrograph, which would generate counter-clockwise hysteresis. In our results, the one clear example of counter-clockwise hysteresis on the falling limb of event 2008b (Figures 2e and 2k, insert) occurs ~ten days after the peak ground vibrations in a typhoon, during an interval, as explained above, when armoring is inferred to have occurred. The peak discharge of the subevent is much smaller than the large typhoons and has less energy to completely destroy the armor on the rising limb. Thus, whereas on the scale of an entire typhoon, net bed armoring may occur, high frequency subevents may introduce complexity that interrupts this trend over shorter timescales.

[19] Other factors may also affect the amplitude of the high frequency seismic noise observed at this site. Although the seismometer is most sensitive to the seismic waves generated proximally, signals are also generated from the more distant reaches. We have adopted the most natural explanation based on observed stage changes locally, but an exhaustive analysis would require data from the entire river system together with the spatial pattern of the river in relation to the seismometer. Also, tributary inputs of finer sediment, including that from debris flows, may affect the seismic signal. Investigating the influence of tributary inputs is beyond the scope of this paper, but we note that to be the explanatory factor for the observed hysteresis in all of our storms, the tributary input timing and characteristics would need to be relatively similar for all events, and additionally would need to affect the seismic wave amplitude over the duration of the falling limb, which we find unlikely.

[20] Lastly, we note that the river gage is 4.25 km downstream of the seismometer. Because flood waves propagate downstream, this means that peak flows are experienced by the seismometer before the river gage. Additionally, at any time on the rising limb of a flood the seismometer will always experience slightly higher flows than the river gage. On the falling limb, the opposite will be the case. Thus the offset between the seismic and hydrological stations provides another possible explanation for hysteresis. However, at 4.25 km apart and using a possible flood flow velocity of 2–5 m/s, the temporal lag between the seismic and hydrologic data would be between 2125 and 850 seconds (35–14 minutes), which is well below our timestep of one hour. This indicates that hysteresis is also probably not due to the spatial offset between the seismic station and the river gage. Moreover, we note that the duration of the seismically observed peak is shorter than the width of the peak of the discharge, which further suggests that the hysteresis is not due to a simple temporal offset of the signals.

5. Conclusions

[21] We have demonstrated that the event-scale time series of high frequency seismic amplitude, a measure of energy from a river available for geomorphic work, is consistent with a bedload source. Using hourly stage and discharge measurements on a gravel-rich mountain stream, we tested hypotheses to explain the measured high frequency seismic noise by water turbulence or bedload transport. We observed clockwise hysteresis in the seismic amplitude-stage and seismic amplitude-discharge relationships for both aggradational and erosional events, consistent with a bedload sediment source for the seismic noise that is dependent on evolving bed packing conditions. The destruction and reformation of armor over the course of the storm is a natural explanation for the observations. The data are inconsistent with hysteresis driven entirely by turbulent pressure fluctuations. These observations demonstrate the potential of fluvial seismology as a method to detect river bed evolution over storm timescales.

[22] **Acknowledgments.** We thank Hui-Hsuan Kate Chen for help with data and translation for the hydrology data, and acknowledge the BATS (Broadband Array in Taiwan for Seismology) for making their data available through the IRIS Data Management Center. The paper benefited from discussions with Colin Stark.

[23] The Editor thanks the two anonymous reviewers for their assistance in evaluating this paper.

References

Adams, P. N., R. S. Anderson, and J. Revenaugh (2002), Microseismic measurement of wave-energy delivery to a rocky coast, *Geology*, *30*(10), 895–898, doi:10.1130/0091-7613(2002)030<0895:MMOWED>2.0.CO;2.

Aki, K., and P. Richards (2002), *Quantitative Seismology*, Univ. Sci., Sausalito, Calif.

Burtin, A., L. Bollinger, J. Vergne, R. Cattin, and J. L. Nabelek (2008), Spectral analysis of seismic noise induced by rivers: A new tool to monitor spatiotemporal changes in stream hydrodynamics, *J. Geophys. Res.*, *113*, B05301, doi:10.1029/2007JB005034.

Burtin, A., L. Bollinger, R. Cattin, J. Vergne, and J. L. Nabelek (2009), Spatiotemporal sequence of Himalayan debris flow from analysis of high-frequency seismic noise, *J. Geophys. Res.*, *114*, F04009, doi:10.1029/2008JF001198.

Charru, F., H. Mouilleron, and O. Eiff (2004), Erosion and deposition of particles on a bed sheared by a viscous flow, *J. Fluid Mech.*, *519*, 55–80, doi:10.1017/S0022112004001028.

Cole, S. E., S. J. Cronin, S. Sherburn, and V. Manville (2009), Seismic signals of snow-slurry lahars in motion: 25 September 2007, Mt Ruapehu, New Zealand, *Geophys. Res. Lett.*, *36*, L09405, doi:10.1029/2009GL038030.

Deparis, J., D. Jongmans, F. Cotton, L. Baillet, F. Thouvenot, and D. Hantz (2008), Analysis of rock-fall and rock-fall avalanche seismograms in the French Alps, *Bull. Seismol. Soc. Am.*, *98*(4), 1781–1796, doi:10.1785/0120070082.

Favreau, P., A. Mangeney, A. Lucas, G. Crosta, and F. Bouchut (2010), Numerical modeling of landquakes, *Geophys. Res. Lett.*, *37*, L15305, doi:10.1029/2010GL043512.

Goff, J. R., and P. Ashmore (1994), Gravel transport and morphological change in braided Sunwapta River, Alberta, Canada, *Earth Surf. Processes Landforms*, *19*(3), 195–212, doi:10.1002/esp.3290190302.

Govi, M., F. Maraga, and F. Moia (1993), Seismic detectors for continuous bed-load monitoring in a gravel stream, *Hydrol. Sci. J.*, *38*(2), 123–132, doi:10.1080/02626669309492650.

Gran, K. B., and D. R. Montgomery (2005), Spatial and temporal patterns in fluvial recovery following volcanic eruptions: Channel response to basin-wide sediment loading at Mount Pinatubo, Philippines, *Geol. Soc. Am. Bull.*, *117*(1–2), 195–211, doi:10.1130/B25528.1.

LaHusen, R. (2005), Acoustic Flow Monitor System—User Manual, *U.S. Geol. Surv. Open File Rep.*, *02-429*.

Leopold, L. B., and W. W. Emmett (1977), 1976 bedload measurements, East Fork River, Wyoming, *Proc. Natl. Acad. Sci. U. S. A.*, *74*(7), 2644–2648, doi:10.1073/pnas.74.7.2644.

Meyer-Peter, E., and R. Müller (1948), Formulas for bed-load transport, in *Proceedings of the 2nd Meeting of the International Association for Hydraulic Structures Research*, pp. 39–64, Delft, Netherlands.

Moog, D. B., and P. J. Whiting (1998), Annual hysteresis in bed load rating curves, *Water Resour. Res.*, *34*(9), 2393–2399, doi:10.1029/98WR01658.

Reid, I., L. E. Frostick, and J. T. Layman (1985), The incidence and nature of bedload transport during flood flows in coarse-grained alluvial

channels, *Earth Surf. Processes Landforms*, *10*(1), 33–44, doi:10.1002/esp.3290100107.

Suwa, H., J. Akamatsu, and Y. Nagai (2003), Energy radiation by elastic waves from debris flows, in *Proceedings of the 3rd International Conference on Debris-Flow Hazards Mitigation: Mechanics, Prediction, and Assessment*, edited by D. Rickenmann and G. F. Wieczorek, pp. 895–904, Millpress, Rotterdam, Netherlands.

Turowski, J. M., A. Badoux, and D. Rickenmann (2011), Start and end of bedload transport in gravel-bed streams, *Geophys. Res. Lett.*, *38*, L04401, doi:10.1029/2010GL046558.

Vilajosana, I., E. Surinach, G. Khazaradze, and P. Gauer (2007), Snow avalanche energy estimation from seismic signal analysis, *Cold Reg. Sci. Technol.*, *50*(1–3), 72–85, doi:10.1016/j.coldregions.2007.03.007.

Water Resources Planning Commission (2008), Hydrological year book of Taiwan, Republic of China, technical report, Minist. of Econ. Aff., Taipei.

Water Resources Planning Commission (2009), Hydrological year book of Taiwan, Republic of China, technical report, Minist. of Econ. Aff., Taipei.

Wilcock, P. R., and J. C. Crowe (2003), Surface-based transport model for mixed-size sediment, *J. Hydraul. Eng.*, *129*(2), 120–128, doi:10.1061/(ASCE)0733-9429(2003)129:2(120).

E. E. Brodsky and N. J. Finnegan, Department of Earth and Planetary Sciences, University of California, Santa Cruz, CA 95064, USA.

L. Hsu, Lamont-Doherty Earth Observatory, 61 Rte. 9W, Palisades, NY 10964, USA. (hsu.leslie@gmail.com)